

# CFRP strengthening of continuous RC T-beams at hogging moment zone across the flange

Mohammad Mohie Eldin<sup>\*1</sup>, Ahmed M. Tarabia<sup>2</sup> and Rahma F. Hasson<sup>3</sup>

<sup>1</sup>Department of Civil Engineering, Faculty of Engineering, Beni-Suef University, Egypt

<sup>2</sup>Department of Structural Engineering, Faculty of Engineering, Alexandria University, Egypt

<sup>3</sup>Department of Civil Engineering, Faculty of Engineering, Sirte University, Libya

(Received January 23, 2017, Revised August 28, 2017, Accepted September 6, 2017)

**Abstract.** Carbon Fiber Reinforced Polymer (CFRP) laminates are used widely either for repairing or strengthening of existing structures. When CFRP laminates are used for strengthening of RC continuous T-beams in the Hogging Moment Zone (HMZ); above and around the intermediate supports, it is important to study the expected positions of the laminates across the width of the beam flange. Although, it is traditional to consider CFRP laminates added above the beam web, this is not practical since walls and columns are located in such positions in general. This paper examines the effect of changing the positions of CFRP laminates used for the strengthening of the hogging moment zone across the beam flange of two-span-T-section beams. The Finite Element (FE) Package ANSYS is used to create 3-D theoretical models needed for the study. It can be concluded that changing the position of CFRP strengthening across the beam flange, in the hogging moment zone, is effective upon the overall behavior. The best locations are either above the web or at the flange just beside the web, due to the presence of walls and/or columns.

**Keywords:** CFRP; continuous beam; RC; ANSYS; strengthening; hogging moment; position; flange

## 1. Introduction

Only little literature is available considering the behavior of two-span continuous beams with rectangular sections strengthened using CFRP laminates. Experimentally and theoretically, an external strengthening of RC beams using bonded CFRP laminates leads to a significant increasing in their ultimate strength (Saleh and Barem 2013). Also, moment redistribution in such beams is possible if the longitudinal and transverse reinforcement configuration is chosen properly (El-Mogy *et al.* 2013). Increasing the number of CFRP layers (not beyond its optimum value) increases both flexure and shear strength and capacity. However, it decreases ductility, moment redistribution, and ultimate strain on CFRP laminates (El-Refaie *et al.* 2003, Maghsoudi and Bengar 2009, Shrestha 2014). Extending the CFRP length to cover the entire hogging or sagging zones did not prevent peeling failure of the CFRP laminates (El-Refaie *et al.* 2003). It was shown that the debonding mechanisms are governed by shear forces and moment redistribution occurring in multi-span beams (Taerwe *et al.* 2009). Adding to these, end anchorage techniques of CFRP laminates were found effective upon the response of reinforced high strength concrete (RHSC) continuous beams (Maghsoudi and Bengar 2009).

Also, Saribiyik and Caglar (2016) concluded that wrapping methods of CFRP laminates affect the behavior of

strengthened beams in terms of flexural strength, ductility and energy absorption capacity. One of the important effects of CFRP strengthening is to restrict the rotation of plastic hinges at their locations, and allow additional plastic hinges formation in unstrengthened cross-sections (Taerwe *et al.* 2009).

On the other side, T-beams are very important since they take into account the interaction between both beams and slabs. However, very rare research is available about T-section simple or continuous beams strengthened using CFRP laminates. Rahman and Rahman (2013) presented an effective technique of applying CFRP laminate for strengthening the hogging zone of continuous T-beam considering column constrains.

The target of this paper is to determine the most proper positions for CFRP laminates across the flange of T-section continuous beams in the hogging moment zone.

## 2. Verification of FE modeling

FE model used in this paper was verified using beam (S2-0); a part of the experimental testing made by Aiello and Ombres (2011) as shown in Fig. 1. Two CFRP strips at sagging region were used and CFRP *U*-jacketing was used at equal distances.

### 2.1 Finite element modeling

#### 2.1.1 Element types

The finite element software ANSYS is used for modeling. Five types of finite elements that support

\*Corresponding author, Ph.D.

E-mail: [mohammad\\_mohie\\_eldin@yahoo.com](mailto:mohammad_mohie_eldin@yahoo.com)

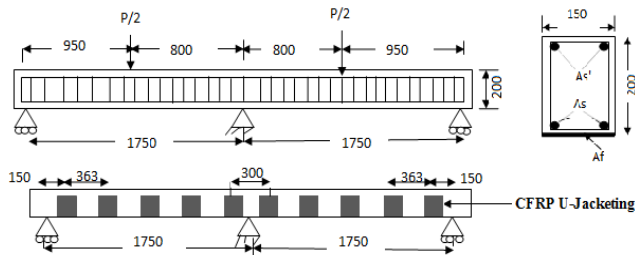
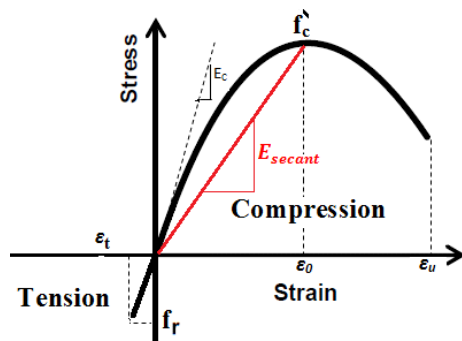
Fig. 1 Details of beam (S2-0) - (Aiello *et al.* 2011)

Fig. 2 Typical RC stress-strain curve

plasticity, large deflection, and large strain capabilities; SOLID65, LINK180, SHELL181, CONTA173, and TARGET170 are used for 3-D modeling of the tested beams, as follows:

- *SOLID65* is defined by eight nodes with three translational degrees of freedom at each node. The solid element is capable of cracking in tension and crushing in compression. It is used for modeling concrete elements.
- *LINK180* is a uniaxial tension-compression element with three translational degrees of freedom at each node. It is used for modeling steel reinforcement bars and stirrups.
- *SHELL181* is a 4-noded element with six degrees of freedom at each node: translations in the  $x$ ,  $y$ , and  $z$  directions, and rotations about the  $x$ ,  $y$ , and  $z$ -axes. As it may be used for layered applications for modeling laminated composite, it is used for modeling CFRP laminates.
- *CONTA173* is a 3-D contact element that is used to represent contact and sliding between “target” surface and a deformable contact surface.
- *TARGE170* is a 3-D target element that is used to represent 3-D “target” surfaces for the associated contact elements (CONTA173).

Target surface is the surface of concrete beam and the deformable contact surface is that of CFRP laminates. Both contact and target elements form what is called “Contact Pair”. The used type of contact pairs is “initially bonded” which allows sliding, gap or both between the two surfaces.

### 2.1.2 Material properties

**Concrete:** Stress-strain curve of concrete is modeled using the equations of Thorenfeldt *et al.* (1987). These equations are mainly functions in the value of the compression strength of concrete ( $f_c$ ). Fig. 2 shows a typical RC stress-strain curve. Additional concrete material

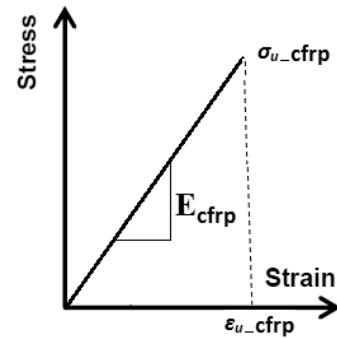


Fig. 3 Typical CFRP stress-strain curve

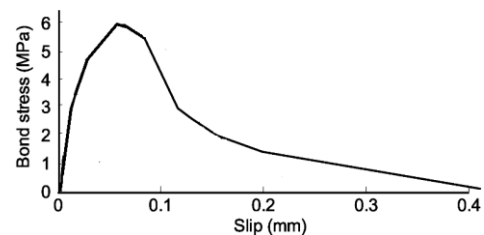


Fig. 4 Local bond stress versus bond slip

data related to SOLID65 element have to be input; shear transfer coefficients and tensile stresses. Shear transfer coefficients range from 0.0 (representing a smooth crack or complete loss of shear transfer) to 1.0 (representing a rough crack or no loss of shear transfer). This specification may be made for both open and closed crack. Shear coefficients of open-cracks and closed-cracks are taken as 0.1 and 0.9, respectively. The modulus of rupture ( $f_r$ ) is taken as 10-15% of the compression strength.

When the element is cracked or crushed, a small amount of stiffness is added to the element for numerical stability. However, crushing capability was turned off to allow convergence of the models. Finally, Poisson’s ratio is taken as 0.2.

**Steel:** Bilinear isotropic material is used to represent the stress-strain curve of steel bars. Required data are Modulus of elasticity ( $E_s = 200,000$  MPa), Poisson’s ratio ( $\nu_s = 0.3$ ), and yield stress ( $\sigma_y$ ).

**CFRP:** Stress-strain curve of CFRP laminates is linear till maximum stress and then dropped to zero stress at maximum strain as shown in Fig. 3. The most appropriate model that can simulate this behavior, accurately, in ANSYS is the multilinear isotropic material.

**FRP-Concrete Interface (Epoxy)** is modeled using a cohesive zone model (CZM) based on tractions and critical fracture energies to provide debonding properties. This failure criteria considers six major parameters; maximum normal contact stress, critical fracture energy for normal separation, maximum equivalent tangential contact stress, critical fracture energy for tangential slip, artificial damping coefficient, and flag for tangential slip under compressive normal contact stress. Since debonding occurs due to shear failure, the first two parameters were not considered. The other four parameters are  $6 \text{ N/mm}^2$ ,  $0.75 \text{ N/mm}$ , 0.1, and 1, according to an experimental bond-slip curve by Lu *et al.* (2005), as shown in Fig. 4.

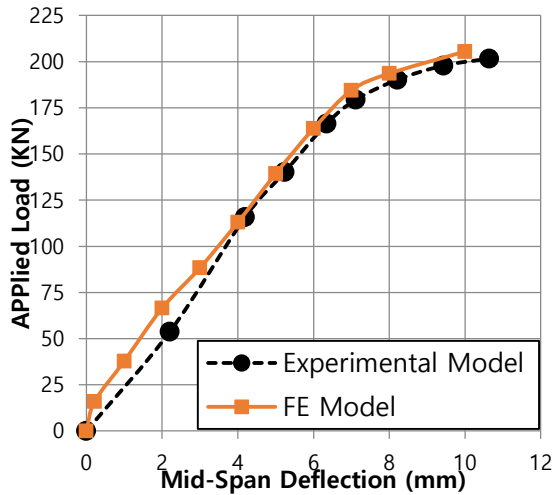


Fig. 5 Experimental and FE results of beam (S2-0)

### 2.1.3 Meshing

A convergence study was done to obtain the acceptable size of solid elements that leads to accurate results in a minimum time. As a result, element size of: ( $x \times y \times z = 50 \times 50 \times 50$  mm) was chosen.

### 2.2 Boundary conditions

The outer two supports are modeled as roller supports to only allow the movement in the direction of the beam axis ( $Z$ ), while the mid-support is pinned support to prevent it from movement in any direction. Due to symmetry, only one quarter of the beam is modeled using the proper boundary conditions at planes of symmetry.

### 2.3 Results

Fig. 5 shows both experimental and FE load-deflection curves of beam (S2-0). The curves show very good agreement that insures using ANSYS as a modeling tool for

continuous RC beams strengthened using CFRP as follows: Ultimate loads are 205.452 and 201.630KN due to FE and experimental results, respectively, with a difference of 1.89%. Maximum deflections are 10 and 10.64 mm due to FE and experimental results, respectively, with a difference of -6%.

## 3. Parametric study

### 3.1 Dimensions of modeled beams

A continuous beam of two spans and T-cross-section is used for the parametric study, as shown in Fig. 6. Each span is loaded by two concentrated loads ( $P$ ) at third and two thirds of the span length. Such beam is subjected to sagging moment along spans and hogging moment at the interior support, as shown in Fig. 7. It is obvious that the length of the hogging moment zone (HMZ) equals  $(3/4 L_1)$  or 1500 mm for each of the two spans. The beam was designed using the Egyptian Code of Practice ECP-203 (2007). The Egyptian Code ECP-208 (2005) was used to obtain the suitable thickness of the CFRP laminates which was approximated to 0.9 mm. However, the designed upper reinforcement at the hogging moment zone was reduced by 75% from (4-bars  $\phi 24$  mm) to (4-bars  $\phi 12$  mm) to allow good investigation of the effect of CFRP strengthening laminates in this zone. CFRP laminate has width equals to the web width (300 mm) and its length equals  $(2L_{CFRP})$  where  $(L_{CFRP})$  is the CFRP length measured from the mid-support. Two lengths were used; 600 mm (short laminate) and 1200 mm (long laminate). Finally, Table 1 shows the mechanical properties of the used materials; concrete, steel, and CFRP.

### 3.2 Effect of the positions of CFRP laminates across the flange

Different locations across the flange are studied to determine the most suitable and practical location for CFRP

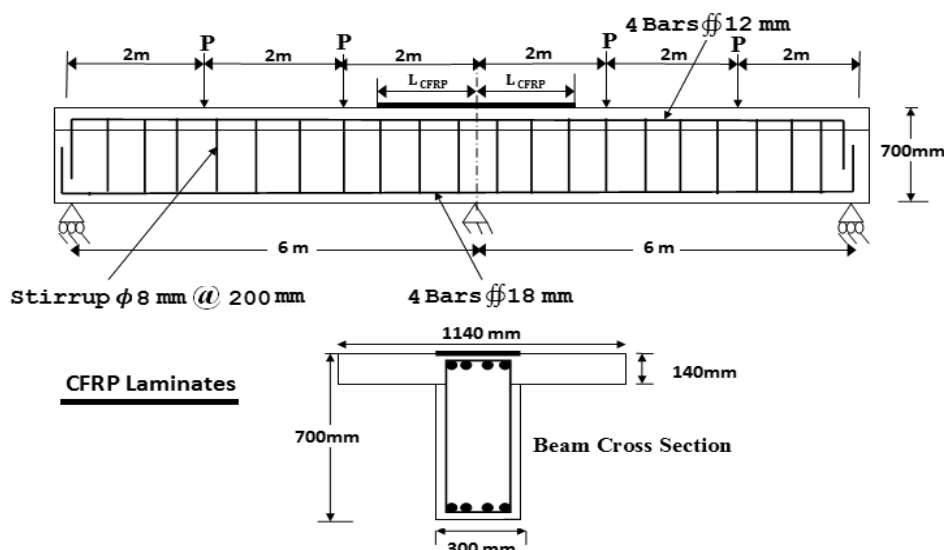


Fig. 6 Dimensions and reinforcement of the modeled beam

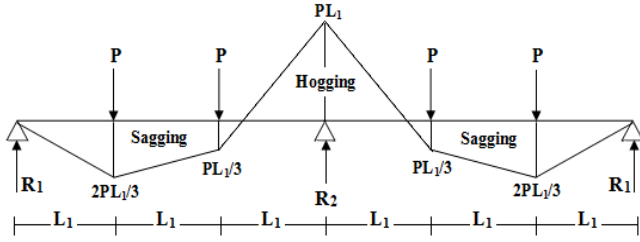


Fig. 7 Bending moment diagram of the modeled beam

Table 1 Mechanical properties of materials

Concrete (MPa)		Steel Bras (MPa)		CFRP Laminates (MPa)		
$f_c$	$f_r$	$E_c$	$f_y$	$E_s$	$\sigma_{u-CFRP}$	$E_{CFRP}$
30	3	26000	400	200000	3050	165000

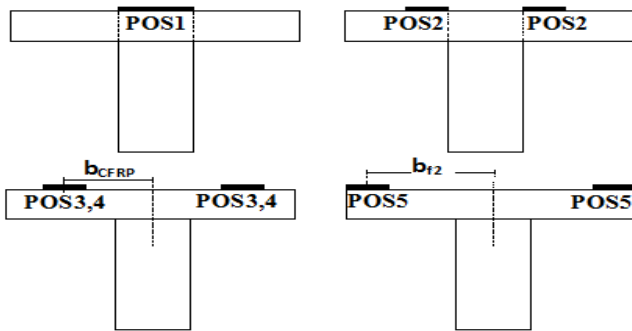


Fig. 8 Positions of laminates across the flange

Table 2 Positions of CFRP laminate

Position	$\frac{b_{CFRP}}{b_{F2}}$	$\frac{L_{CFRP}}{=0.4 L_{HMZ}} = 600 \text{ mm}$	$\frac{L_{CFRP}}{=0.8 L_{HMZ}} = 1200 \text{ mm}$	CFRP Width (mm)	Location
POS1	0	√	√	300	On the Web
POS2	0.45	√	√	2×150	Beginning of the Flange
POS3	0.55	√	√	2×150	Across the Flange
POS4	0.90	√	√	2×150	Across the Flange
POS5	1	√	√	2×150	End of the Flange

laminates. For each location, two lengths for CFRP laminates are used; ( $0.80L_{HMZ} = 1200 \text{ mm}$ ), and ( $0.40L_{HMZ} = 600 \text{ mm}$ ) to examine if there is an interaction between the position of the laminate and its length. The details are shown in Fig. 8 and Table 2.

### 3.3 Results and discussions

#### 3.3.1 Load - deflection results

Fig. 9 and Tables 3 and 4 show load-deflection results for both control (unstrengthened) and strengthened beams of CFRP lengths 600 and 1200 mm. It is shown that repositioning the laminates from web towards flange ends decreases both capacity and deflection of the beam. The maximum percentage of decreasing in both the ultimate applied load ( $\Delta P$  %) and deflections ( $\Delta \delta$  %) are

$$\Delta P \% = \frac{P - P_{POS1}}{P_{POS1}} \% \quad (1)$$

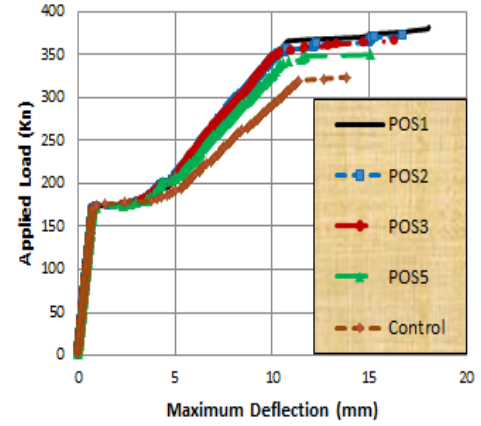
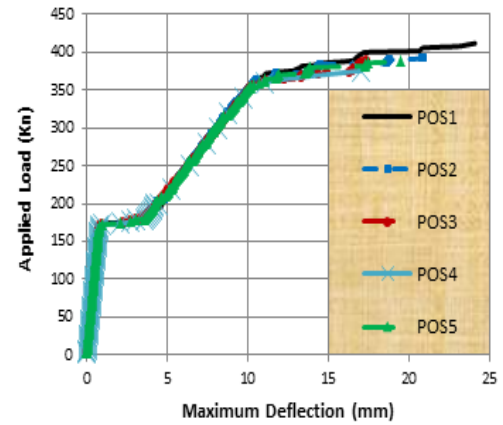
(a)  $L = 0.40 L_{HMZ}$ (b)  $L = 0.80 L_{HMZ}$ 

Fig. 9 Load-deflection curves

Table 3 Load-deflection results for CFRP length 600 mm

Location	$L_{CFRP} = 600 \text{ mm}$				
	Deflection (mm)	Maximum Load (KN)	$\Delta \delta$ %	$\Delta P$ %	Failure Mode
POS1	18	376	----	-----	CFRP Debonding
POS2	16.7	370	-7.22	-1.6	CFRP Debonding
POS3	16.3	363	-9.44	-3.4	CFRP Debonding
POS4	15.5	354	-13.8	-5.8	CFRP Debonding
POS5	15.1	350	-16.1	-6.9	CFRP Debonding

$$\Delta \delta \% = \frac{\delta - \delta_{POS1}}{\delta_{POS1}} \% \quad (2)$$

The values of maximum decreasing of the ultimate load (and maximum deflections) are 6.9% (16.1%) and 8.3% (32.4%) for lengths 600 and 1200 mm, respectively.

#### 3.3.2 Stresses of CFRP laminates at different stages of loadings

Figs. 10 to 12 show the distribution of stresses in CFRP laminates along their lengths at different stages of loadings for lengths 600 and 1200 mm. Strains are distributed in the same manner as stresses due to the elastic behavior of the CFRP laminates. Table 5 shows the maximum CFRP

Table 4 Load-deflection results for CFRP length 1200 mm

Location	$L_{CFRP}=1200$ mm				Failure Mode
	Deflection (mm)	Maximum Load (KN)	$\Delta\delta\%$	$\Delta P\%$	
POS1	24.1	420	----	----	Crushing of Concrete at Mid-Support
POS2	20.9	406	-13.28	-3.3	Crushing of Concrete at Mid-Support
POS3	19.6	398	-18.67	-5.2	Crushing of Concrete at Mid-Support
POS4	16.5	386	-31.54	-8.1	Crushing of Concrete at Mid-Support
POS5	16.3	385	-32.37	-8.3	Crushing of Concrete at Mid-Support

stresses at failure for the different locations and their percentages comparing with POS1. According to the results and as a general, stresses decrease with repositioning of the laminates from web towards the ends of the flange. The worst position is POS5; at the ends of the flange for which the stresses are much less than other locations which means minimum utilization of the CFRP laminates.

Whatever the location of the strengthening, stresses are gradual. For 1200 mm length, the stresses at the ends of the laminates are approximately zero which expresses good transition of stresses without concentration. This is not the case for 600 mm length. Also, it is seen that the stresses in

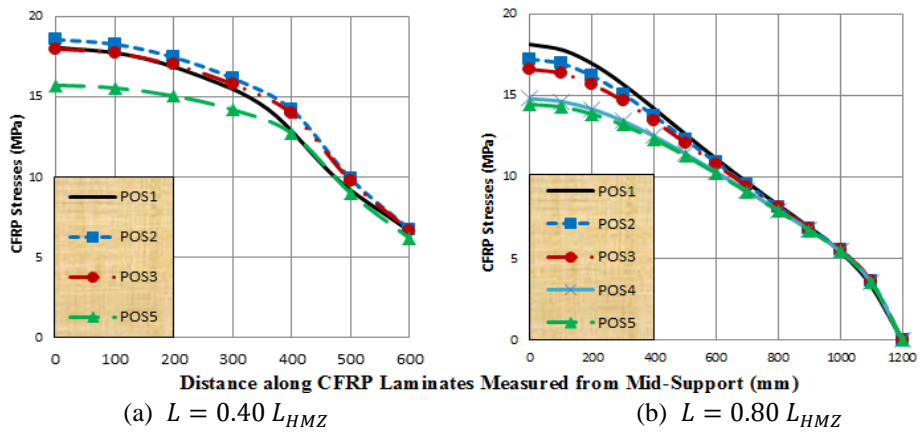


Fig. 10 CFRP stresses at first crack

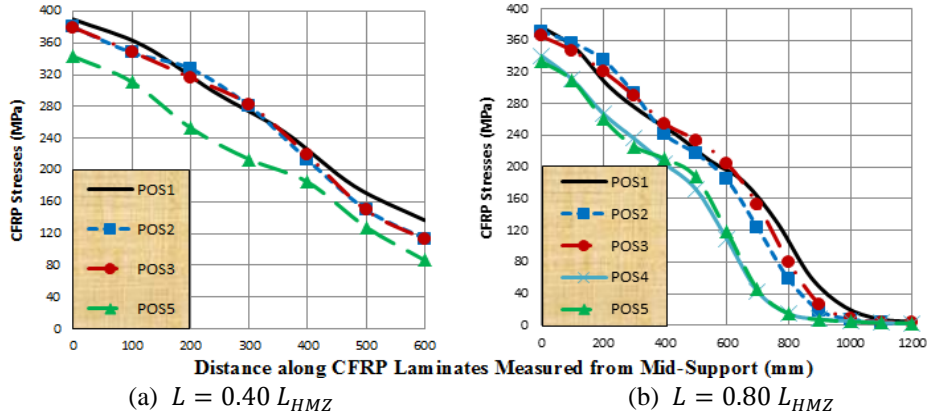


Fig. 11 CFRP stresses at yielding of upper steel

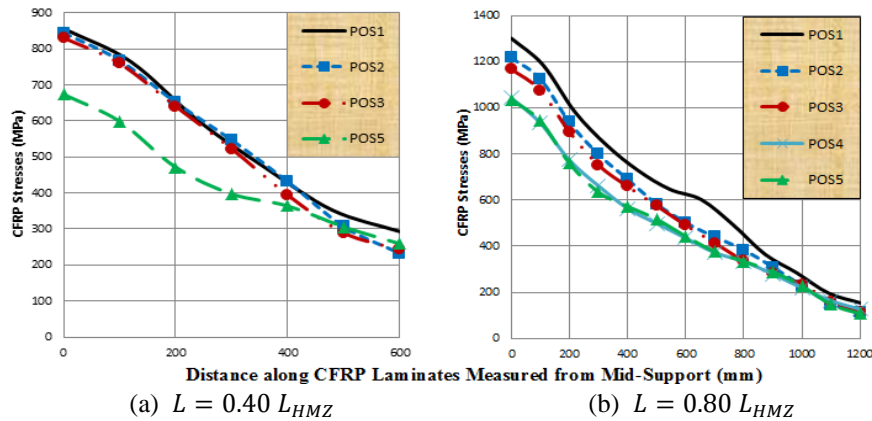


Fig. 12 CFRP stresses at failure

Table 5 Maximum CFRP stresses

Location	POS1		POS2		POS3		POS4		POS5	
	$\sigma_{u-CFRP}$	$\sigma_{u-CFRP}$ %								
$L_{CFRP}=600$ mm	856.94	845.18	98.63	831.33	97.01	701.34	81.84	674.37	78.70	
$L_{CFRP}=1200$ mm	1302.4	1217	93.44	1168.5	89.72	1037	79.62	1034	79.39	

both lengths are approximately equal until upper steel yielding. This means that the effects of both the location and the length of the CFRP laminate begin after yielding of steel. Finally, according to Fig. 12, only about 40% of the

CFRP capacity is reached. An explanation of this behavior is that the beams are designed to fail in flexure; enough CFRP thickness.

3.3.3 Stresses/strains of steel bars at different stages of loadings

Figs. 13 to 16 show the distribution of stresses and strains of upper steel bars along their lengths at different stages of loadings for lengths 600 mm ( $L = 0.40 L_{HMZ}$ ) and 1200 mm ( $L = 0.80 L_{HMZ}$ ). Table 6 shows the maximum strains of upper steel bars at failure for the different positions of CFRP laminates and their percentages comparing with POS1.

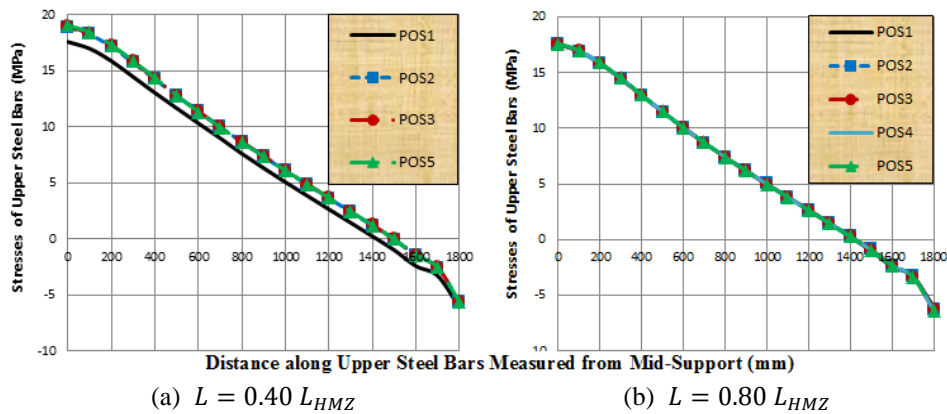


Fig. 13 Stresses in upper steel bars at first crack

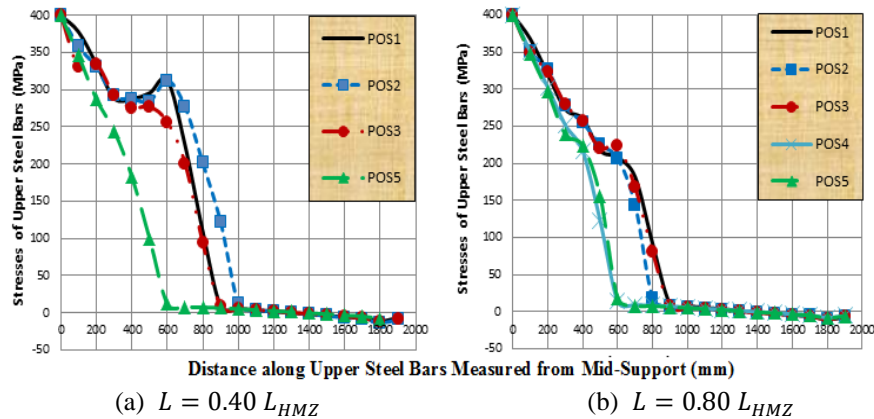


Fig. 14 Stresses in upper steel bars at yielding of steel

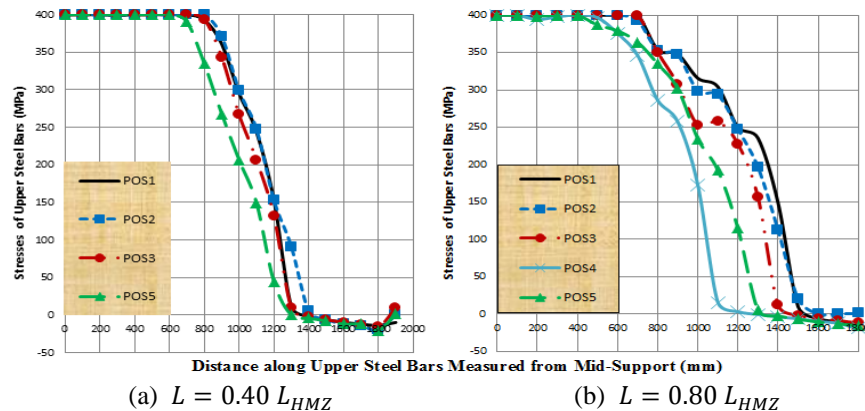


Fig. 15 Stresses in upper steel bars at failure

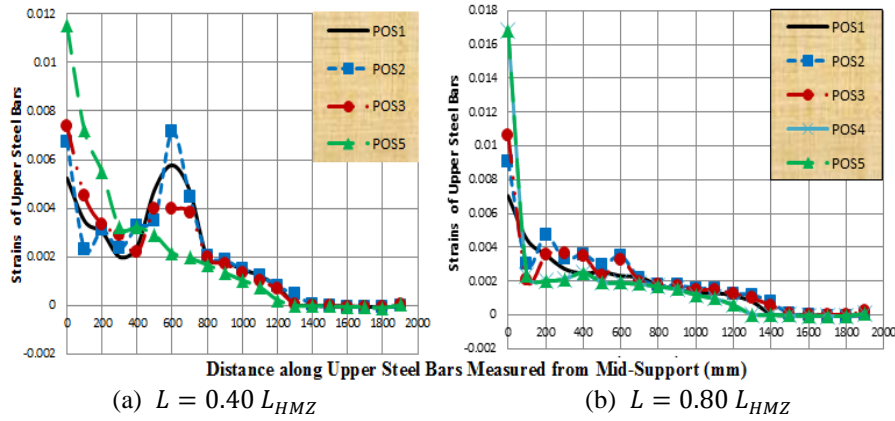


Fig. 16 Strains in upper steel bars at failure

Table 6 Steel strains at failure

Location	POS1		POS2		POS3		POS4		POS5	
	$\epsilon_{u-CFRP}$	$\epsilon_{u-CFRP}$	%	$\epsilon_{u-CFRP}$	%	$\epsilon_{u-CFRP}$	%	$\epsilon_{u-CFRP}$	%	$\epsilon_{u-CFRP}$
$L_{CFRP}=600$ mm	.00523	.00676	129.3	.00738	141.1	0.0115	219.9	.0115	219.9	9
$L_{CFRP}=1200$ mm	.00703	.00906	128.9	.0107	152.2	.0168	238.9	.0168	238.9	

Table 7 Moment redistribution factor ( $\beta$ ) for length 600 mm

Position of CFRP	$P_u$ (KN)	Reactions (KN)		Mid-Support			Span		
		Mid-Support	End Support	$M_{FE}$ (KN.m)	$M_E$ (KN.m)	$\beta$ (%)	$M_{FE}$ (KN.m)	$M_E$ (KN.m)	$\beta$ (%)
POS1	376	237.88	138.12	299.28	376	20.4	276.24	250.66	10.2
POS2	370	233.8	136.20	292.8	370	20.8	272.4	246.66	10.4
POS3	366	230.74	135.26	286.44	366	21.74	270.52	244.00	10.86
POS4	354	218.80	135.20	250.8	354	29.15	270.4	236	14.5
POS5	350	215.80	134.20	244.80	350	30.06	268.40	233.33	15.03
Control	326	189.91	136.09	162.00	326	50.31	272.18	217.00	25.43

Table 8 Moment redistribution factor ( $\beta$ ) for length 1200 mm

Position of CFRP	$P_u$ (KN)	Reactions (KN)		Mid-Support			Span		
		Mid-Support	End Support	$M_{FE}$ (KN.m)	$M_E$ (KN.m)	$\beta$ (%)	$M_{FE}$ (KN.m)	$M_E$ (KN.m)	$\beta$ (%)
POS1	420	279.45	140.55	416.7	420	0.78	281.1	280	0.39
POS2	406	268.44	137.56	393	406	3.2	275.12	270.66	1.64
POS3	398	251.34	136.16	377	398	5.27	272.33	265.33	2.63
POS4	386	240.24	135.76	343	386	11.13	271.52	257.33	5.5
POS5	385	240.2	135.8	340.2	385	11.6	271.6	256.66	5.8
Control	326	189.91	136.09	162.00	326	50.31	272.18	217.00	25.43

According to the results, the following may be concluded:

1. Stress distribution of upper steel bars at failure consists of three parts. The first is located in the vicinity of the mid-support at which the stress is maximum and equals to steel strength. The second is located in the mid-CFRP-length at which going away from the web decreases the stresses which means less utilizing of steel bars. The third part is located at the end of the laminate at which the stress is minimum with a value in zero limits.

2. Strains, at mid-support region, increase with moving away the web. Strains of POS5 at failure increase by about 220 and 240% for lengths 600 and 1200, respectively, comparing with POS1. This insures that repositioning the laminates away the web, especially at the ends of the flange, leads to great softening (decreasing the utilization) of the upper steel bars.

Positioning of the laminates away from the web decreases the concentration of strains in steel bars at the end of the short CFRP laminates (600 mm length).

### 3.3.4 Moment redistribution

In this section, redistribution of moments between both sagging and hogging moments is examined. This redistribution allows good utilizing of the beam capacity. Moment redistribution factor ( $\beta$ ) is defined as

$$\beta = \frac{|M_{FE} - M_E|}{|M_E|} \times 100 \quad \% \quad (3)$$

$M_{FE}$  is the bending moment calculated from FE results at failure (using both failure loads and their corresponding reactions), and  $M_E$  is the failure bending moment calculated elastically due to failure load, as follows

$$M_{FE-Hogging} = 3L_1(R_1 - P) \quad (4)$$

$$M_{FE-Sagging} = R_1L_1 \quad (5)$$

$$M_{E-Hogging} = PL_1 \quad (6)$$

$$M_{E-Sagging} = 2PL_1/3 \quad (7)$$

Where:  $P$  = the applied point load at failure,  $R_1$  = the reaction of the external support at failure, and  $L_1$  = one third of the span length, as shown in Fig. 7.

Tables 7 and 8 and Fig. 17 show the values of the redistribution ratio ( $\beta$ ) of both sagging (span) and hogging (mid-support) moments for different positions of CFRP laminates for lengths 600mm ( $L = 0.40 L_{HMZ}$ ) and 1200 mm ( $L = 0.80 L_{HMZ}$ ), respectively.

According to the previous results:

- Moment redistribution factor ( $\beta$ ) increases with repositioning of the laminates away from the web. The maximum increasing occurs when CFRP laminate is put at the ends of the flange.

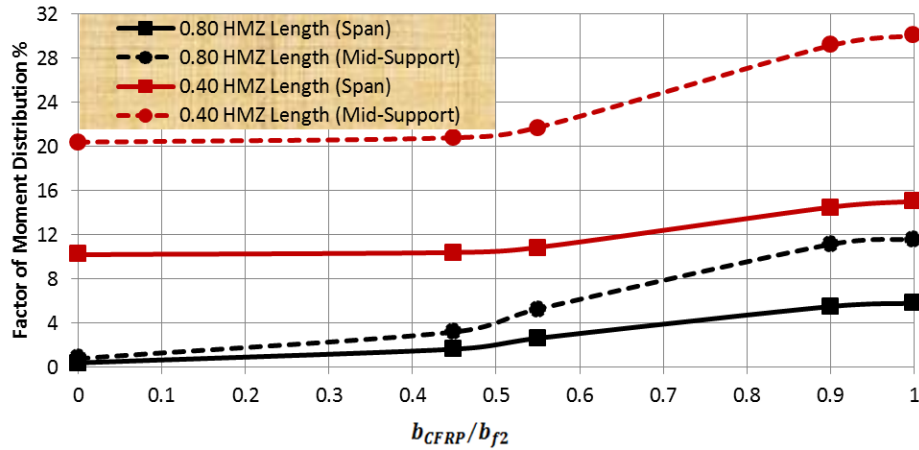


Fig. 17 Factor of moment redistribution ( $\beta$ ) as a function of the laminate position

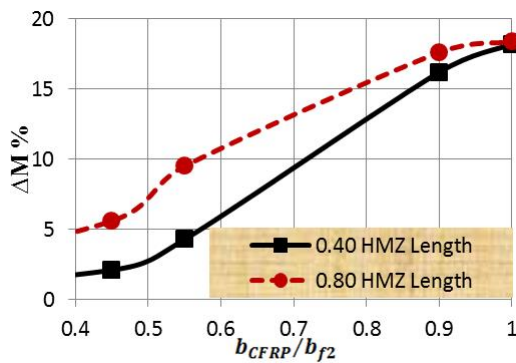


Fig. 18 Percentage of negative moment reduction along beam flange

Table 9 Percentage of moment decreasing related to the position located at the web

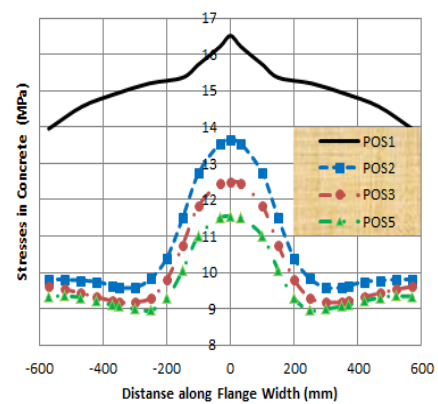
Position of CFRP	CFRP Length=0.4 $L_{HMZ}=600$ mm			CFRP Length=0.8 $L_{HMZ}=1200$ mm		
	$P_u$ (KN)	$M_{FE}$ (KN.m)	$\Delta M$ %	$P_u$ (KN)	$M_{FE}$ (KN.m)	$\Delta M$ %
POS1	376	299.28	-----	420	416.7	-----
POS2	370	292.8	-2.1	406	393	-5.6
POS3	366	286.44	-4.29	398	377	-9.5
POS4	354	250.8	-16.2	386	343	-17.6
POS5	350	244.80	-18.2	385	340.2	-18.36

- Hogging moment (at the central support) decreases with repositioning of CFRP laminates away from the web- axis towards the ends of the flange. Fig. 18 and Table 9 show the percentage of this decreasing ( $\Delta M$  %) for the different positions related to the position located at the web, where

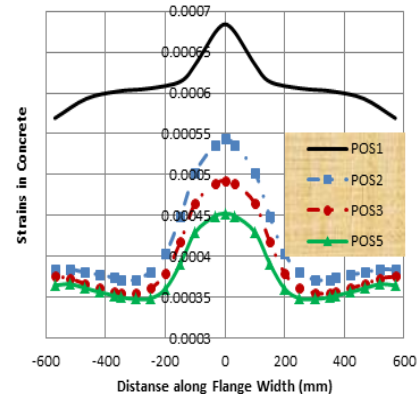
$$\Delta M \% = \left( \frac{M_{POS} - M_{POS1}}{M_{POS1}} \right) \times 100 \quad \% \quad (8)$$

### 3.3.5 Stresses/strains in concrete

In this section, stresses and strains of concrete at either mid-span or mid-support are studied. Fig. 19 shows concrete stresses and strains, respectively, for different positions at failure. It is shown that there is a considerable



(a) Stresses



(b) Strains

Fig. 19 Concrete compression stresses/strains at mid-span at failure for different positions of the laminate

difference in concrete stresses between putting CFRP laminates above the web and above the flange. However, going away from the web decreases both stresses and strains which means less utilizing of concrete.

Fig. 20 shows stresses and strains, respectively, of concrete in compression zone (bottom of the web) at mid-support at different stages of loading when CFRP laminates are above the web (POS1). Stress and strain values at failure are  $\geq 30$  MPa and 0.0034, respectively, which are the maximum input values. This means that failure occurs in the compression zone (web bottom) at mid-support

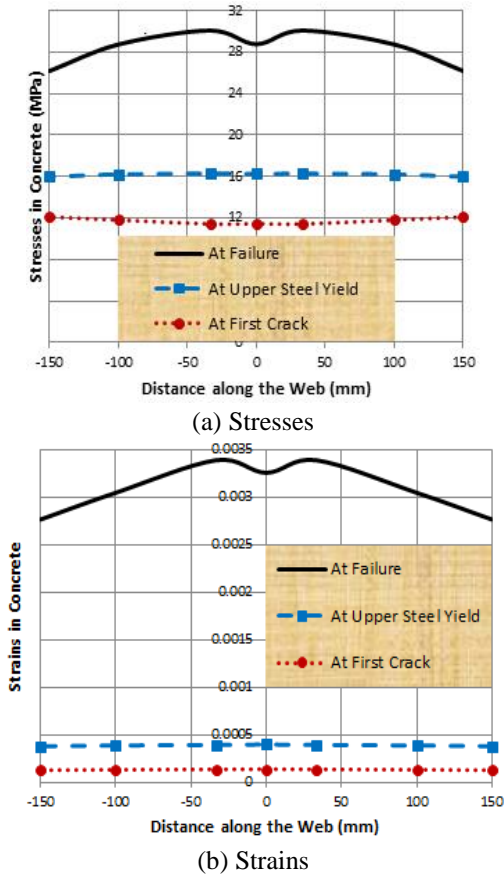


Fig. 20 Concrete compression stresses/strains at support for POS1

according to crushing of concrete not to debonding of CFRP laminates. This is logic since beams were designed to allow crushing of concrete not debonding of CFRP laminates to examine only the change of their positions. Fig. 21 shows failure compression stresses and strains, respectively, in concrete at mid-support at the bottom of the web. Failure may occur if either the stress or the strain reaches its maximum allowable value. This is the reason that failure stresses are not equal as shown in Fig. 21(a). However, the values for all the positions are very close. This means that the presence of CFRP laminates at the top of the beam flange, in the mid-support region, only affects the concrete stresses / strains at the top of the beam flange, in mid-span region.

### 3.3.6 Failure mechanisms

The steps of forming a failure mechanism with continuing of applying loading:

- The upper reinforcement at the mid-support reaches the yield.
- Due to the presence of the CFRP, no plastic hinge will form in the mid-support region (at the upper reinforcement).
- The lower reinforcement in the span reaches the yield.
- A plastic hinge is formed in the location of the maximum positive moment.
- Moment redistribution between positive and negative

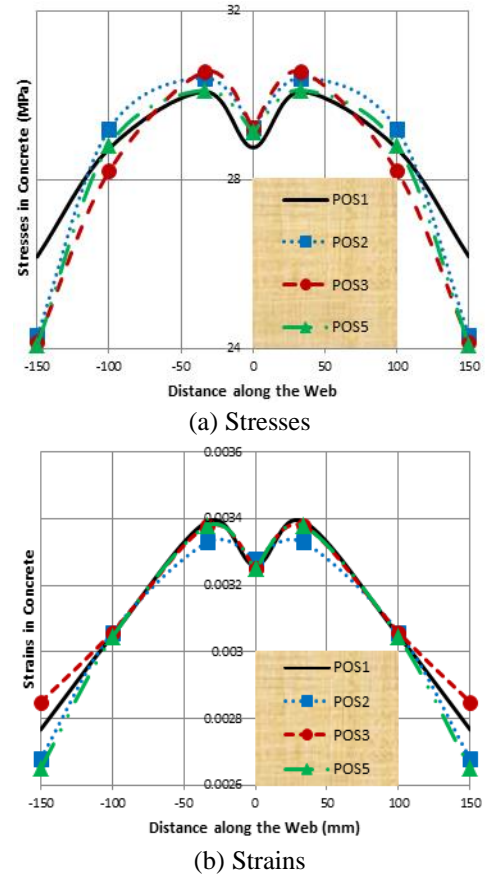


Fig. 21 Concrete compression stresses/strains at support at failure

moments begins.

vi. Negative moment increases till failure in two ways:

- For long CFRP laminates, the failure mode is concrete crushing at the mid-support.
- For short CFRP laminates. The failure mode is debonding between the CFRP laminates and the concrete surface.

## 4. Conclusions

This paper examines the effect of varying the locations of CFRP laminates used for the strengthening of the hogging moment zone across the flange of T-beams, using the ANSYS FE Package. According to the obtained results, repositioning of CFRP laminates away from the web:

- Decreases moment capacity either sagging or hogging.
- Decreases maximum deflection and, as a consequence, ductility.
- Decreases CFRP stresses and, as a consequence, strains.
- Increases strains in upper steel bars, in the vicinity of the mid-support, by more than 200%, which means a great amount of softening.
- Decreases the concentration of strains in upper steel bars at the end of short CFRP laminates, while steel strains transmit smoothly for long CFRP laminates whatever the CFRP position.

- Decreases the stresses in upper steel bars in the mid-length of the CFRP laminate, at failure, while these stresses equal steel strength in the vicinity of the mid-support and approximately equal zero in the end-part of the CFRP laminate.
  - Decreases both concrete stresses and strains in the mid-span region which means less utilizing of concrete.
- Adding to the previous conclusions:
- Moment redistribution factor is maximum at the ends of the flange while it is minimum at the web.
  - Putting CFRP laminates above the web gives much more utilizing of the concrete compression strength/strain than other positions.
  - The presence of CFRP laminates at the top of the beam flange, in the mid-support region, only affects the concrete stresses / strains at the top of the beam flange, in mid-span region.
  - The disadvantages of putting the CFRP laminate away from the web increases with increasing the laminate length.
  - Whatever the position of the CFRP laminate, failure modes are “concrete crushing at the mid-support” and “debonding between the CFRP laminates and the concrete surface” for long and short laminates, respectively.

As a conclusion, putting CFRP laminates over the web (POS1) is the best position for CFRP strengthening laminates if there are no walls above the web. If there is a wall above the web, the best location is to put the CFRP laminates at both sides of the (web) wall. These positions utilize perfectly steel bars, concrete and CFRP laminates.

## References

- Aiello, M.A. and Ombres, L. (2011), “Moment redistribution in continuous fiber-reinforced polymer-strengthened reinforced concrete beams”, *ACI Struct. J.*, **108**(2), 158-166.
- ANSYS (2013), “ANSYS Help”, Release 15.0.
- ECP-203 (2007), Egyptian Code of Practice for the Design and Implementation of Reinforced Concrete Structures, Housing and Building Research Center (HBRC), Cairo, Egypt.
- ECP-208 (2005), Egyptian Code for the Design Principles and Implementation Requirements of Using CFRP in Fields of Construction, Housing and Building Research Center (HBRC), Cairo, Egypt.
- El-Mogy, M., El-Ragaby, A. and El-Salakawy, E. (2013), “Experimental testing and finite element modeling on continuous concrete beams reinforced with fibre reinforced polymer bars and stirrups”, *Can. J. Civil Eng.*, **40**(11), 1091-1102.
- El-Refaie, S.A., Ashour, A.F. and Garrity, S.W. (2003), “Sagging and hogging strengthening of continuous reinforced concrete beams using carbon fiber-reinforced polymer laminates”, *ACI Struct. J.*, **100**(4), 446-453.
- Iesa, W.M., Alferjani, M.B.S., Ali, N. and AbdulSamad, A.A. (2010), “Study on shear strengthening of RC continuous beams with different CFRP wrapping schemes”, *Int. J. Integ. Eng.*, **2**(2), 35-43.
- Lu, X.Z., Ten, J.G., Ye, L.P. and Jaing, J.J. (2005), “Bond-slip models for FRP sheets/plates bonded to concrete”, *J. Eng. Struct.*, **24**(5), 920-937.
- Maghsoudi, A.A. and Bengar, H.A. (2009), “Moment redistribution and ductility of RHSC continuous beams strengthened with CFRP”, *Turkish J. Eng. Environ. Sci.*, **33**, 45-59.
- Rahman, M.M. and Rahman, M.W. (2013), “Simplified method of strengthening RC continuous T beam in the hogging zone using carbon fiber reinforced polymer laminate-A numerical investigation”, *J. Civil Eng. Constr. Technol.*, **4**(6), 174-183.
- Sakr, M.A., Khalifa, T.M. and Mansour, W.N. (2014), “External strengthening of RC continuous beams using FRP plates: finite element model”, *Proceedings of the Second Intl. Conf. on Advances in Civil, Structural and Mechanical Engineering-CSM 2014*, 168-174.
- Saleh, A.R. and Barem, A.A.H. (2013), “Experimental and theoretical analysis for behavior of R.C. continuous beams strengthened by CFRP laminates”, *J. Babylon Uni. (Iraq), Eng. Sci.*, **21**(5), 1555-1567.
- Saribiyik, A. and Caglar, N. (2016), “Flexural strengthening of RC beams with low-strength concrete using GFRP and CFRP”, *Struct. Eng. Mech.*, **58** (5), 825-845.
- Shrestha, U.S. (2014), “Modified composite application to improve strength and ductility of structural components”, MSc Dissertation, College of Graduate Studies, The University of Toledo, Ohio, United States.
- Taerwe, L., Vasseur, L. and Matthys, S. (2009), “External strengthening of continuous beams with CFRP”, *Concrete Repair, Rehabilitation and Retrofitting II*, London.
- Thorenfeldt, E., Tomaszewicz, A. and Jensen, J. (1987), “Mechanical properties of high strength concrete and application to design”, *Proceedings of the Symposium: Utilization of High-Strength Concrete*, Stavanger, Norway, June.

CC